Convective Chimneys and Plumes in the Northern Greenland Sea

Ola M. Johannessen,[1,2,3] Kjetil Lygre[1] and Tor Eldevik[1,4]

In the Boreas Basin in the northern Greenland Sea, convection has been observed to be localized as narrow structures—chimneys—in which the water masses may be homogeneous from the surface through great depths. An experiment was carried out in the area by R/V *Håkon Mosby* of the University of Bergen with an aim to detect and investigate chimneys, their structure, and the inherent convective plumes. A chimney was detected at 77.5°N, 0.5°E, by towing an undulating conductivity–temperature–depth (CTD) profiler (Seasoar). Complementary deep CTD stations taken as close as 2.5 km apart, revealed that the chimney was about 30 km in the zonal and 15 km in the meridional directions. The mixed-layer depth inside the chimney was about 500 m, indicating that the chimney was of an upper ocean type. Deep convection was improbable because of the modest cooling of a culminating winter. The Seasoar tows within the chimney revealed weak horizontal temperature, salinity, and density anomalies of 1-5 km extent, i.e. of the order of the internal Rossby deformation radius. Similar scales were characteristic of a nonhydrostatic ocean model set up accordingly. The CTD sections also revealed enhanced sea surface density within cyclonic rim eddies with a diameter of the order of 5 km. Wavelet spectra of the horizontal temperature variability inside the core of the chimney revealed increased power on the 100-m scale, which is of the same magnitude as a plume scale determined from theoretical studies. This is the first time such a plume scale has been directly derived from high-resolution (~10 cm) horizontal CTD (Seasoar) measurements alone.

INTRODUCTION

During the past few decades the understanding of the links between mesoscale (O(1-10 km)) dynamics and the global circulation through deep water formation has been a key area of ocean science. A central phenomenon is the *chimney* process [MEDOC-group, 1970], in which active deep convection takes place within a spatially limited area. Its mechanisms have been reviewed in detail by Marshall and Schott [1999], who further claimed that little *net* vertical mass flux takes place inside a chimney and therefore recommended that the term "mixed patch" should be used instead. In the present article, however, we will adhere to the original terminology in accord with the MEDOC-group [1970].

Although the detailed mechanisms of the chimney process remain unknown, chimneys have been observed during wintertime in the weakly stratified waters of the Mediterranean, Labrador, and Weddell seas [*Gascard*, 1991], as well as the Greenland and Boreas basins [*Johannessen et al.*, 1991]. In synthesizing all available observations on chimneys until then, *Gascard* [1991] aimed at a more precise definition of their characteristics. There is now a general agreement that a chimney goes through three main stages. First, there is

[1]Nansen Environmental and Remote Sensing Center, Bergen, Norway.
[2]Geophysical Institute, University of Bergen, Norway.
[3]Mohn-Sverdrup Center for Global Ocean Studies and Operational Oceanography, Bergen, Norway.
[4]Bjerknes Centre for Climate Research, Bergen, Norway.

XXXXX
Geophysical Monograph Series XXX

10.1029/XXXGMXX

a preconditioning phase in which the intermediate water is brought to the surface [*Killworth*, 1979]. The triggering mechanism may be baroclinic instability of the mean flow, a topographically induced perturbation, or ice edge upwelling [*Johannessen et al.*, 1983]. Second, there has to be strong forcing (cooling) at the surface in order to convert the intermediate water to deep water by buoyancy loss. A substantial part of the cooled, dense water overturns as plumes with a horizontal scale of the order of 100 m, before rapid mixing of the properties of the plumes is forming a homogeneous mixed patch, tens of kilometers in horizontal extent [*Marshall and Schott*, 1999]. The final stage, decay, involves baroclinic instability of the rim current of the chimney [*Send and Marshall*, 1995], manifested as rim eddies with diameters of the order of the internal Rossby radius of deformation. Numerical model experiments by *Send and Marshall* [1995] showed that the rim features are organized as several smaller cyclones, or *cones*, propagating away from the chimney and thus dispersing properties away from the generation area.

There has recently, however, been a shift in focus from the gyre-scale mixed patch of *Marshall and Schott* [1999] back to the mesoscale chimney and its associated dynamics, e.g., *Gascard et al.*, [2002]. The chimney concept of *Killworth* [1979] is consistent with the recent emphasis that it is the ocean "preconditioning" (as opposed to anomalies in the atmospheric forcing) that mainly localizes convection [*Legg and Marshall*, 1993; *Straneo and Kawase*, 1999]. Also, for the last decade or so there has been no sign of gyre-scale overturning in the Greenland Sea [*Watson et al.*, 1999; *Alekseev et al.*, 2001, 2003]. Ventilated water has instead been associated with pronounced mesoscale eddies of about 5-km radius [*Gascard et al.*, 2002; *Wadhams et al.*, 2002]. In agreement with this scenario such eddies were generated in the numerical model ocean of *Eldevik and Drange* [2002]. This is also consistent with Killworth's model [*Killworth*, 1979], in which chimneys were postulated to be preconditioned by baroclinic instability of the Greenland Sea Gyre rim current. A result of the instability is dense-core, weakly stratified cyclonic eddies. When the gyre region is exposed to wintertime cooling, these anomalies will be prone to convective overturning.

Through several investigations during the Marginal Ice Zone Experiments (MIZEX) campaign, a number of upper ocean chimneys or chimney-like structures were observed and described. During the MIZEX-87 programme in the Boreas Basin [MIZEX-group, 1989; *Sandven et al.*, 1991] structures were typically 10-20 km in diameter, extended from the surface down to about 600 m, and consisted of lower Arctic Intermediate Water (lAIW), which was relatively warm (1.0°C), saline ($S = 34.96$), and dense ($\sigma_\theta = 28.02$) compared to the surrounding water. Two years later during the Seasonal Ice Zone Experiments 89 program [SIZEX group, 1989; *Johannessen et al.*, 1991], a remarkably well-defined chimney containing Deep Water ($T = -0.41$°C, $S = 34.91$) was observed outside the ice edge. It was 20 km in diameter with uniform potential density in the upper 500 m, below which the density increased by only 0.02 sigma-units near bottom at 2800 m. (Hereafter we refer to this as *Chimney89*.)

In order to increase our understanding of chimneys in relation to convective overturning and to characterize the submesoscale and the scale of the plumes within the chimneys, an investigation was carried out in the Boreas Basin in the northern Greenland Sea during February 1994.

In the next section we present the methods and experimental approach. In the third section the observational data are presented together with the results of a nonhydrostatic ocean model. The results are discussed and summarized in the final section.

METHODS AND EXPERIMENTAL LAYOUT

The aim of the R/V *Håkon Mosby* ESOP/CARDEEP[5] experiment in the Boreas Basin during 9-21 February 1994 was to detect chimneys and subsequently describe their structure, scales, and dynamics, including plumes within the chimneys. Whereas previous cruises in the Boreas Basin were more concentrated close to the ice edge [MIZEX-group, 1989; *Johannessen et al.*, 1991], the central part of the basin was the focus of the present investigation. The cruise track is shown in Figure 1. During the initial period of the experiment, the basin was crisscrossed with a towed undulating CTD sensor platform (Seasoar) profiling the upper 200-250 m of the water column, sampling typically every 2.5 km in the horizontal to detect chimneys; these features were further investigated by detailed Seasoar tracks and densely spaced deep CTD casts, to obtain optimal coverage both horizontally and vertically. This is the first time the horizontal structure inside a chimney has been investigated with such high horizontal resolution.

The definition of the detailed experiment centered around 77.5°N, 0.5°E was based on the discovery of a relatively homogeneous, high-density area, subsequently defined as a chimney. It was further investigated first by crisscrossing the site with the Seasoar in a star-patterned grid, followed by a towing of the Seasoar at a fixed depth of 20 m (Figure 2) along 6 zonal legs about 30 km long separated by approximately 4 km, effectively sampling every 10 cm in the horizontal. Hence, the postulated horizontal plume scale of ~100 m would be well resolved. Eventually, 40 CTD casts were taken to 1000 m or near the bottom, with station separation as low as 2.5 km in

[5]European Sub-Polar Ocean Programme/Carbon and Deepwater Formation. Q1

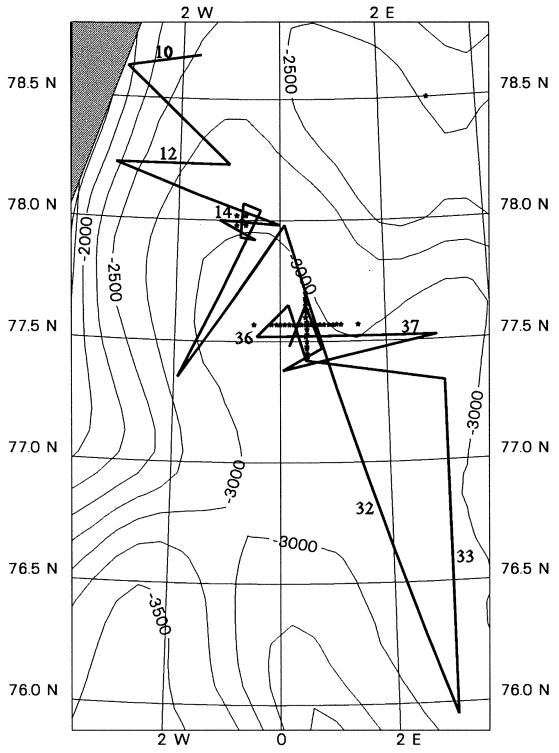

Figure 1. Ship track (lines) with leg numbers referenced in the text, plotted for those tracks on which the Seasoar was vertically profiling the mixed layer down to 250 m. Locations of the deep CTD stations (asterisks) and the ETOPO5 bathymetry (labeled contours) are also shown. The ice edge is indicated in the upper left corner in gray shading.

order to resolve the mesoscale structure of the chimney in the upper part of the ocean. One N–S section was taken along 0.5°E from 77.43°N to 77.7°N, and an E–W section was taken along 77.57°N from 0.5°W to 1.5°E (Figure. 2).

The same Neil Brown Mark III CTD sonde was used both in the Seasoar and deep CTD surveys in order to obtain a consistent data set. Salinity has been computed according to PSS78 [UNESCO, 1983], and about 5 salinity samples were taken on each deep station for calibration purposes. An overall r.m.s. difference between the calibrated CTD and salinometer analysis of $\sim 5 \times 10^{-3}$ was found, sufficiently accurate for this investigation, as our study is focused in the upper 1000 m. Temperature accuracy is about 2×10^{-3} °C. Temperatures θ are hereafter given as referred to surface pressure, which is also the case for the density variable σ_θ, if not otherwise stated. In situ temperature is denoted by T. Except for the fixed-depth tows, all CTD data are averaged over 2 dBar.

A ship-mounted Aanderaa weather station provided standard meteorological parameters from which surface heat flux has been estimated. Furthermore, Synthetic Aperture Radar (SAR) images from the European Space Agency ERS-1 satellite facilitated the determination of characteristic length scales and shapes of the mesoscale structures in the investigation area. A hull-mounted Acoustic Doppler Current Profiler was logging the water velocity. Unfortunately, the quality of navigation information was not good enough to obtain absolute velocities; therefore, these data have been disregarded in the following analysis.

DATA

Before describing the chimney we first provide a brief characterisation of the ambient upper ocean water masses and the mesoscale features captured by the Seasoar profiling, as well as the deep hydrographic structure. We also estimate the turbulent heat flux (the dominant part of the total) to 200 Wm^{-2}. This is based on typical figures for the observed wind speed, 10 m s^{-1}, atmospheric temperature, –10°C, and relative humidity, 75%, logged by the weather station in the mast of the ship, and sea surface temperature of about 0°C. Due to the difficulties in correcting for the effect of the ship on the air flow, we have not considered the details of the temporal evolution of the heat flux.

For the Seasoar we present, for brevity, only surface temperature data; the salinity plots are reported in Johannessen and Lygre [1996], from which the referenced salinity values are taken. From the tracks (Plate 1) it is evident that a major part of the surface water is relatively warm ($T > 0.6$°C) and saline ($S > 34.9$). We will denote this water mass Arctic Surface Water (ASW), even if it is slightly too saline to fit the classical definition of *Carmack* [1990]. In the eastern and northern parts of the area covered by the Seasoar tows there are occurrences of still warmer ($T > 1.5$°C) and saltier ($S > 34.96$) water which apparently is recirculated from the Atlantic domain [*Johannessen et al.*, 1987a,b]; we denote this Atlantic Water (AW). Substantially colder and fresher water masses are found at the boundary of the survey area, north of 78°N and west of 3°W, i.e., Polar Water defining the Polar Front. Similar water masses occur south of 76.3°N in association with the steep southeastward directed topographic ridge—the Greenland Fracture Zone—apparently guiding admixtures of water from the Polar domain into the basin. The Seasoar, limited to span the surface layer, only casually captured the intermediate water masses below the mixed layer (ML).

A Characteristic of the region is the mesoscale variability (Plate 1), including cold and less saline water as well as warm and saline water with several patches on the 5-10-km horizontal scale with AW signatures. The chimney is centered at

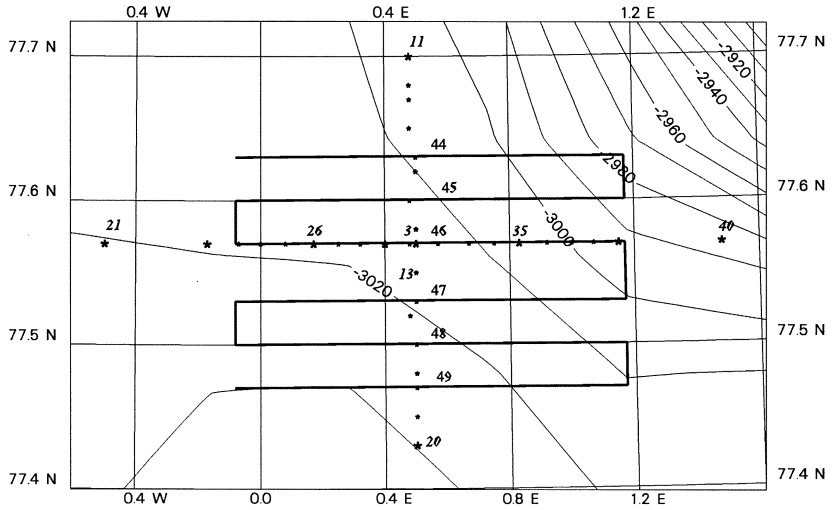

Figure 2. Blow-up of the survey area in the *Chimney94* region. Deep CTD stations are marked with asterisks; smaller symbols indicate 1000 m casts, larger symbols denote casts to near bottom. Station numbers in italics are referenced in other figures. The tracks where the Seasoar was towed at a nominal depth of 20 m are shown with lines; track numbers in normal types. Coarse bathymetry (ETOPO5) is shown as labeled contours.

about 77.55°N, 0.5°E, roughly bounded by the 0.7-0.8°C isotherms, i.e. belonging to the ASW and surrounded by AW eddy-like intrusions. The size of the horizontal features scales well with the Rossby internal deformation radius R_d, estimated by taking numbers from the vertical density profile in Figure 3 as

$$R_d = \frac{N}{f} H \simeq 3 \text{ km}$$

in which N is the buoyancy frequency, f the local Coriolis parameter, and H a vertical scale here equated with the ML depth (500 m). In computing N, the density gradient is computed from σ_1 at 1000 m and at the surface, using UNESCO [1981]. Even if full two-dimensional coverage is not granted for these patches, they are interpreted as eddies, since they are of the order of R_d and eddies are known to be abundant in the area [*Johannessen et al.*, 1987b, 1995].

Providing further detail in the vertical, the deep CTD stations generally reveal that the ML depth is about 500 m (Figure 3) with $\theta \simeq 0.6$°C, $S \simeq 34.93$, below which the temperature and salinity abruptly change to $\theta \simeq -0.2$°C, $S \simeq 34.89$, with a minor density increase. The following 150 m is the layer of largest static stability, in which the density changes 0.015 units over 150 m.

Between the ML base and about 1000 m depth, the salinity is fairly constant (34.89), while a temperature gradient is stabilising with $\theta \simeq -0.7$°C at 1000 m. The temperature then decreases somewhat more slowly while salinity increases to about 34.91 at 1400 m. Even if a temperature minimum is not observed as in the Greenland Gyre [*Budéus*, 1998], this water mass fits approximately to the definition of upper Arctic Intermediate Water (uAIW). Similarly, the underlying water mass is interpreted as lAIW, although no clear property maxima are found around 1000-1500 m. At 3000 m the temperature is down to –1.15°C, with salinity about 34.91, i.e. well-defined Greenland Sea Deep Water. There is also a very weak indication of a salinity maximum around 2300 m, indicating a weak influence of Arctic Ocean Deep Water [*Aagaard et al.*, 1991].

The upper and intermediate waters do not fit precisely into a common water-mass classification [*Carmack*, 1990], which may be no surprise, as the warm, saline influence in the Boreas Basin comes more directly from the Atlantic and Norwegian Sea waters, compared to the Greenland Basin. In particular, the surface water, which was arbitrarily defined as ASW, is close to lAIW characteristics. However, since lAIW is located deeper and apparently isolated from the surface, it is awkward to categorize the surface water as AIW. It can rather be interpreted as a derivative of AW and uAIW.

Chimney94

When inspecting the vertical deep CTD sections taken through the chimney, it is apparent that it can be defined by

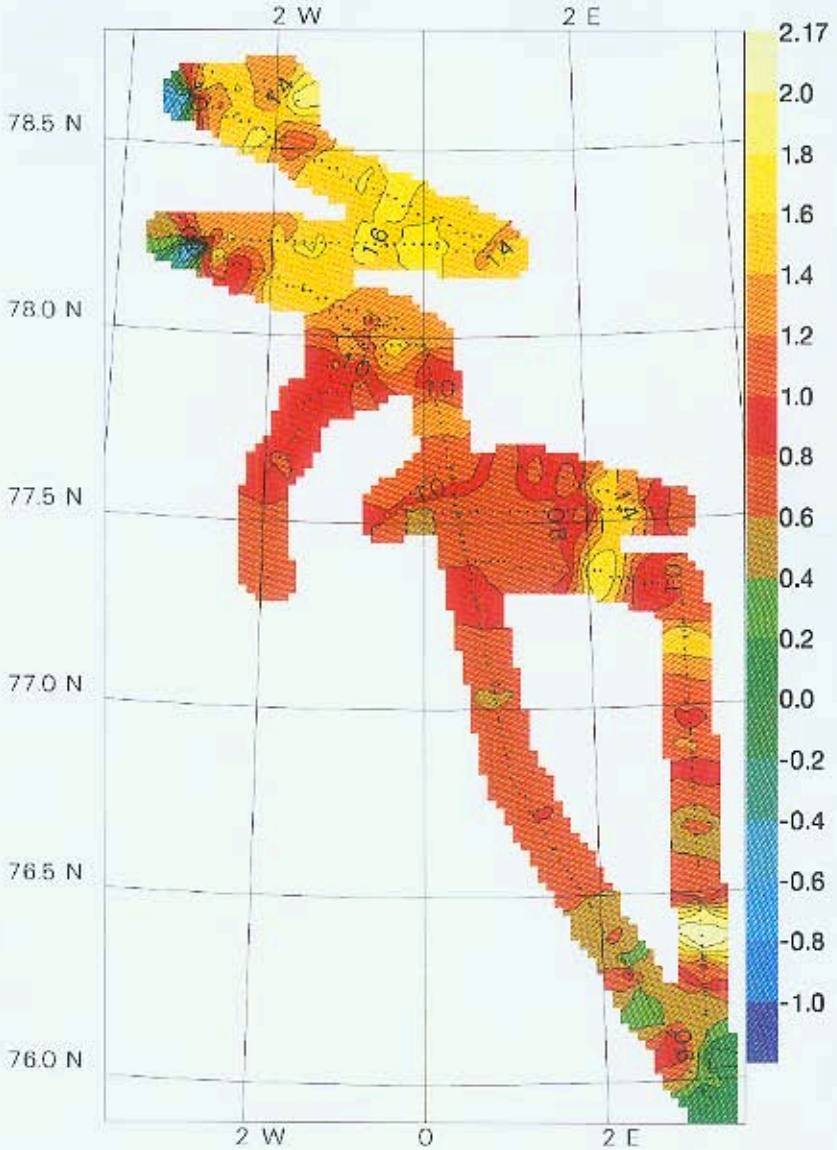

Plate 1. Horizontal plot of near surface (5 m) temperature obtained with the Seasoar on 9-16 Feb. 1994. Temperature scale [°C] to the right; contour interval is 0.2°C. Black dots indicate location of individual profiles, approximately 2.5 km apart.

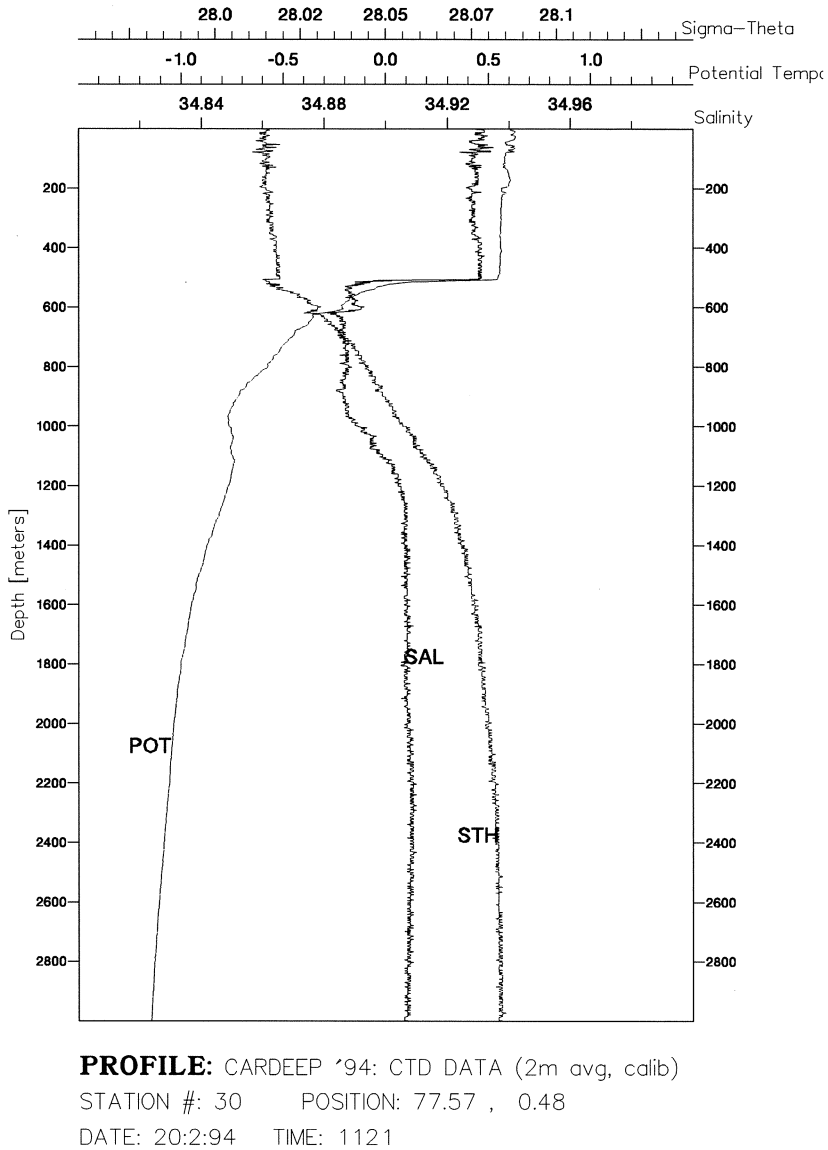

Figure 3. Profiles at station 30 in the center of the chimney. (POT, potential temperature; SAL, salinity; STH, σ_θ).

the fairly homogeneous water mass of the ML, in which salinity is about 34.93, temperature 0.5-0.7°C, and $\sigma_\theta <\simeq 28.02$ sigma-units, with a well-defined boundary towards a warm, saline water mass to the north (Figure 4) and west (Figure 5). The core of the chimney has a north–south and east–west extent of approximately 15 and 30 km, respectively, using the 0.7°C isotherm as a criterion (Figures 4a and 5a). In the southern and eastern parts, the horizontal property gradients are weak, implying a more diffuse transition towards the exterior.

There is also a slight variability within the core, in that the coldest and freshest water appears close to the northern rim (Figures 4a,b between 6 and 10 km). This also corresponds to the densest water ($\sigma_\theta \simeq 28.02$; Figure 4c) with no detectable change over the 500-m-deep ML, consistent with cooling

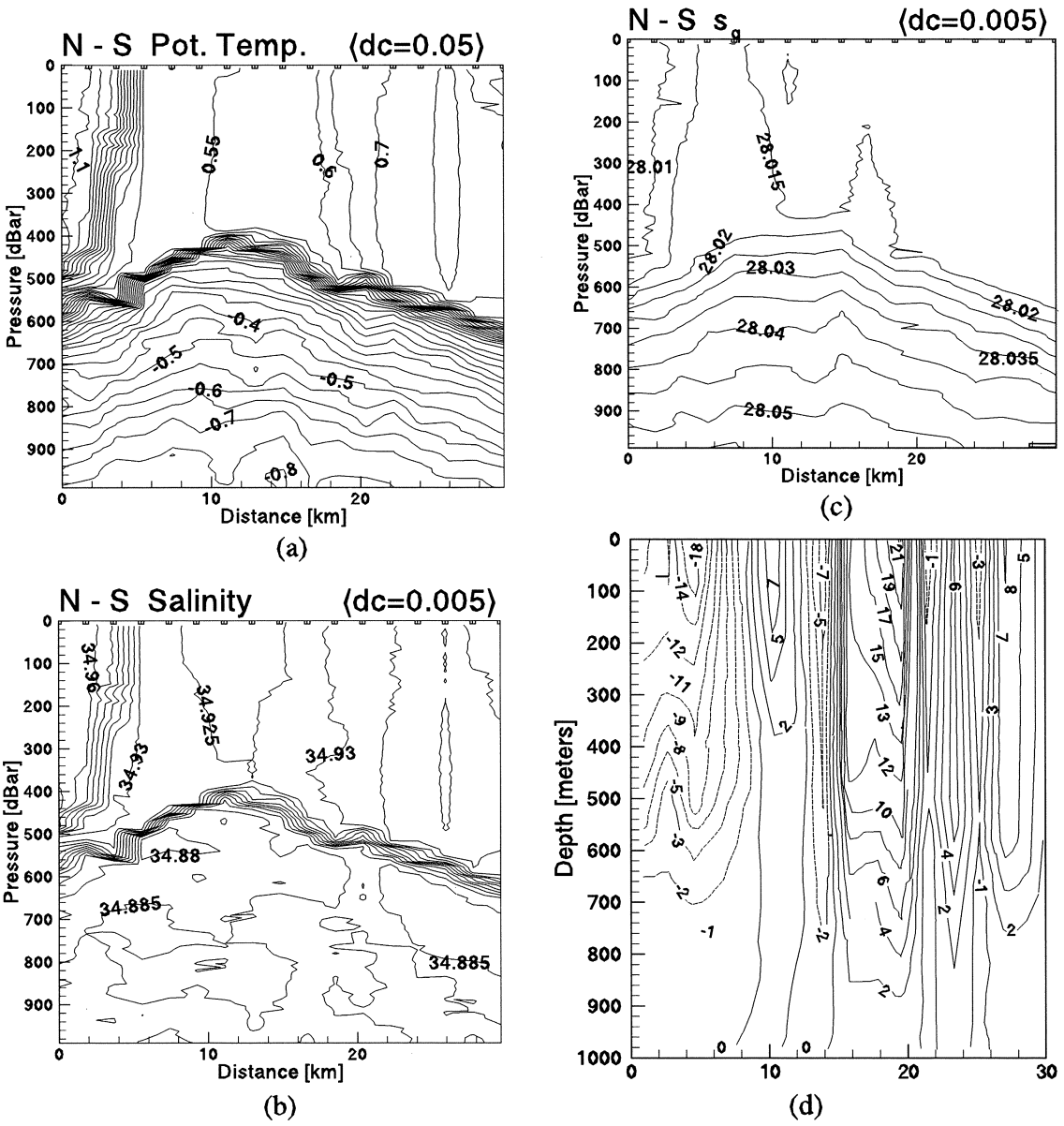

Figure 4. North to south CTD section through the core of chimney of (a) potential temperature, (b) salinity, (c) σ_θ and (d) geostrophic speed [cm s^{-1}] relative to 1000 dBar. Positive current is directed eastward, into the paper. The features between 6 and 10 km and between 10 and 15 km are described in the text.

and buoyancy loss from the surface. Slightly to the south there is a tendency for a weak salinity stratification ($\Delta S \approx 0.01$ over the uppermost 250 m [Figure 4b], between 10 and 15 km), implying a corresponding density stratification (Figure 4c), whereas all other stations further south have changes in ML density less than 0.01 sigma-unit.

The pycnocline (Figure 4c) shows a well-defined dome shape reaching 500 m deep at the center and deepening

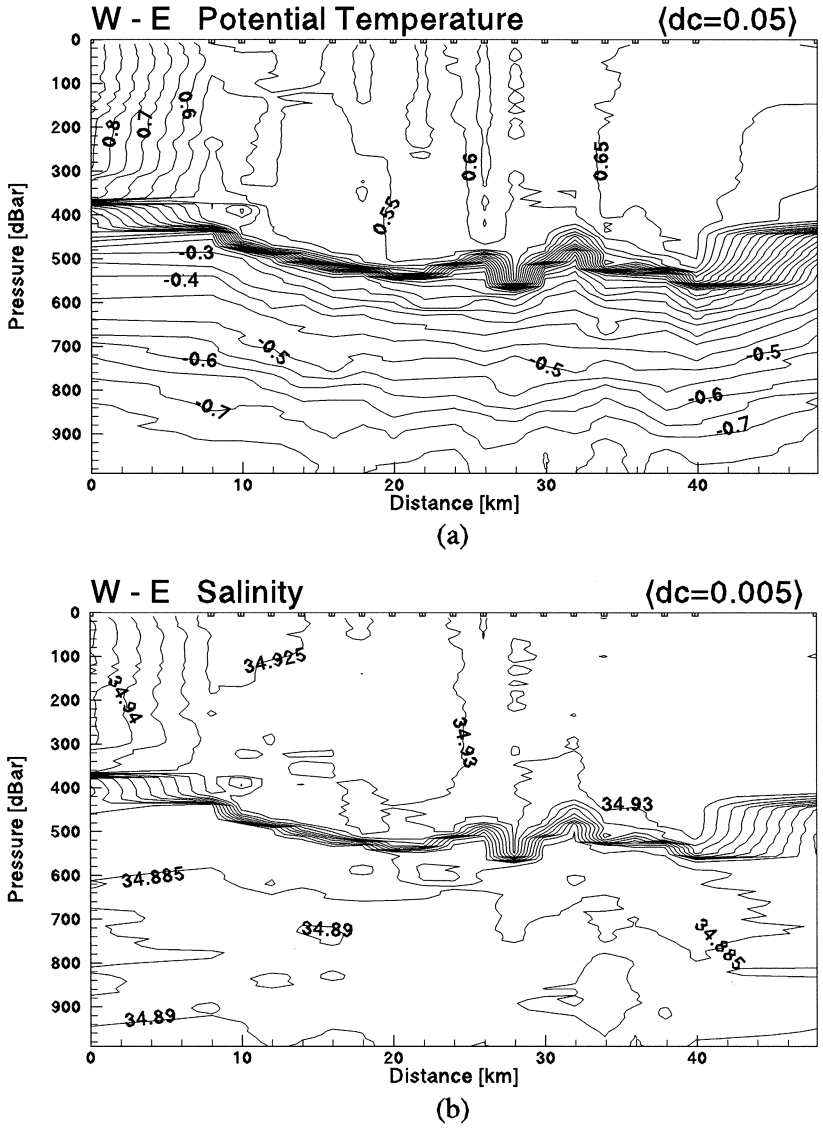

Figure 5. West to east CTD section through the core of chimney of (a) potential temperature, (b) salinity, (c) σ_θ and (d) geostrophic speed [cm s^{-1}] relative to 1000 dBar. Positive current is directed northward, into the paper. The features between 8 and 15 km are described in the text.

to about 600 m at the rim. The implied geostrophic speed (Figure 4d) shows a westward surface intensified jet extending over about 10 km near the northern rim reaching about 18 cm s^{-1}, with a corresponding eastward current covering the following 10 km, i.e. spanning the chimney scale. This well-defined cyclonic shear zone is consistent with a rim current, although there are insufficient data to discern this from a background current. The horizontal shear of the geostrophic current is approximately 2×10^{-5} s^{-1}, which is only one order of magnitude smaller than f. Suffice it to say that the chosen level of no motion is somewhat arbitrary but in agreement with other studies in the area, e.g., *Johannessen* [1987a].

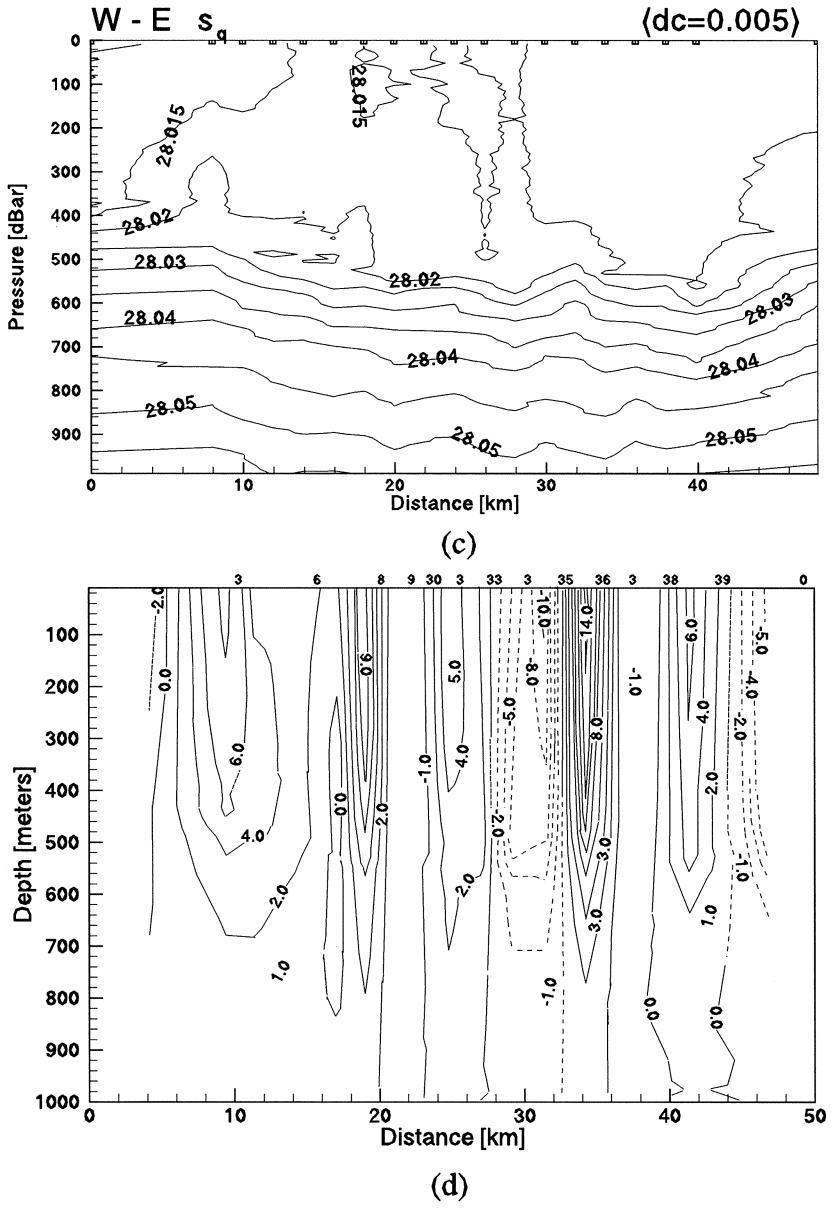

Figure 5. (Continued).

Elevating it to 500 m would reduce the horizontal shear by roughly 50%. Furthermore, the same authors showed that the barotropic velocities can be considerable, especially over steep bottom features. However, as we are focusing on upper ocean features on the 10-km scale and smaller in an area of modest topographic variability, the geostrophic current should be fairly representative.

As the scale of the current system (20 km) is much larger than R_d (= 3 km), the condition for baroclinic instability is met [*Pedlosky*, 1979]. For the horizontal structure of

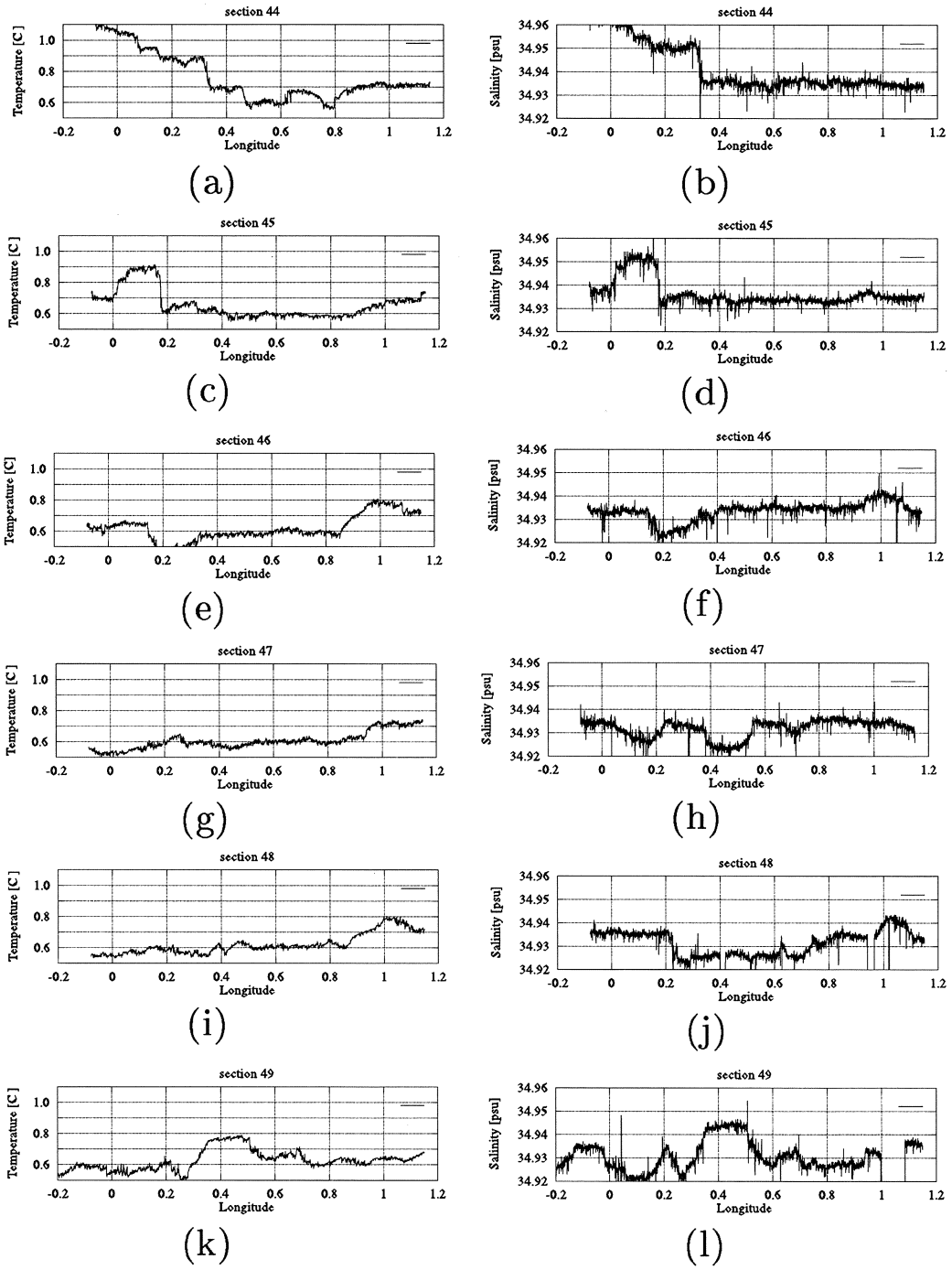

Figure 7. Along-track distribution of in situ temperature (left) and salinity (right) from the legs where the Seasoar was towed in ~20 m. The data have been reduced from ~10 cm horizontal resolution to ~10 m, by taking consecutive medians.

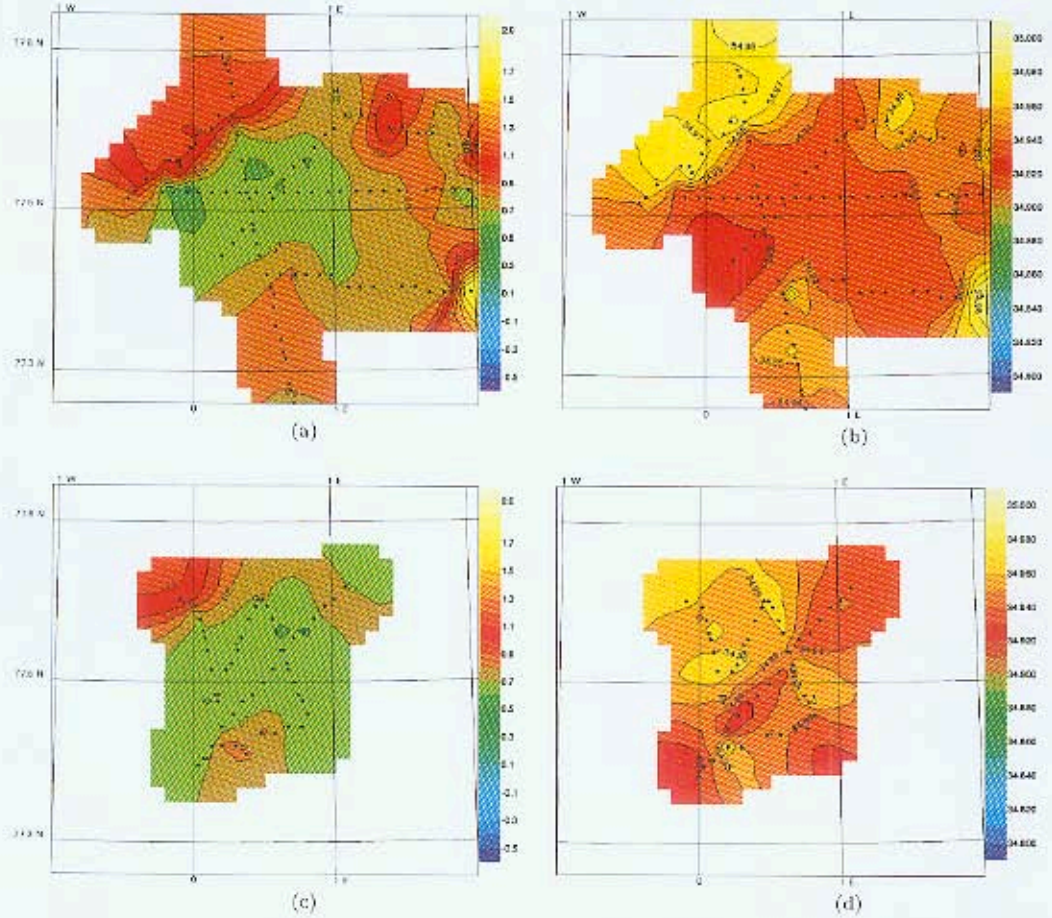

Plate 2. Blow-up of the *Chimney94* area, showing (a,c) temperature and (b,d) salinity. (a) and (b) maps were obtained over 3.5 days, while (c) and (d) were derived from the final 6 hours of the survey, immediately following the former. Contour interval is 0.1°C for temperature and 0.01 for salinity.

the geostrophic current, variability on the kilometer scale should be interpreted with caution, since the separation is comparable to R_d, not to mention the nonsynopticity. It is not obvious if there is an inflection point in the chimney-scale horizontal velocity profile, the criterion for barotropic instability [*Pedlosky*, 1979]. Baroclinic instability thus seems to be the most likely generation mechanism for the rim eddies, in agreement with *Send and Marshall* [1995].

As mentioned above, also on the E–W section the core water of the chimney is slightly colder (by less than 0.05°C) and fresher near the rim than in the center (Figures 5a,b, between 8 and 15 km from the west). Again, the density displays a maximum in the same area (Figure 5c, at about 15 km). The relatively fresh water near the surface (between 8 and 15 km) suggests enhanced contact with the fresh pycnocline layer by slightly enhanced convective mixing perhaps in combination with the elevated pycnocline near the rim.

The pycnocline (Figure 5c) is generally more leveled out in comparison to the N–S section, or even has a slight bowl shape, most markedly on the sides. The relatively steep inclination of the pycnocline to the west gives rise to a maximum northward geostrophic speed of about 6 cm s^{-1} in Figure 5d. Besides from somewhat lower speed, there was no well defined cyclonic circulations like that seen on the N–S section.

Mesoscale Structure

The most detailed synoptic map of the near-surface structure of the chimney is that obtained from the 20-m-deep tows. For a better view of its rim we first inspect the last crisscrossings with the undulating Seasoar (Plate 2). Again defining the core as enclosed by the 0.7°C contour, the core apparently extends about 15 km in the meridional and 30 km in the zonal directions, as also seen on the CTD sections. The region to the east of 1°E is apparently very patchy, with eddy-like structures of less than 10 km extent, both cold/fresh and warm/saline anomalies. In the lower right corner in Plates 2a,b resides the warm core and saline anticyclonic feature previously discussed in relation to Plate 1. Its vertical structure appears clearly on Seasoar Section 37 (Figure 1) along 77.52°N (Figure 6; descends 627-634). It is about 15 km in diameter and shaped as a lens, as is characteristic for upper ocean anticyclones. Warm, saline AW is also found in the northwestern part of the chimney, bounded by a front (Plates 2a,b), again consistent with the previous information from the deep sections. Similarly, the minimum of temperature and salinity just inside the chimney core is also evident.

It is also revealed that the temporal variability is significant. When comparing Plates 2a,b from several days of profiling with the final 6 h, (Plates 2c,d), it is seen that synopticity cannot be granted, e.g., the northwestern front has moved northwards. The final Seasoar crisscrossing reinforced the previous overall view of the area with respect to temperature (compare Plates 2a and c), although the spatial range was somewhat smaller. Temporal variability is also evident on closer inspection of CTD stations 1, 12, and 30, i.e. those taken at the same location (77.57°N, 0.5°E) separated by time intervals of 13.5 and 29 h, respectively (not shown). In between stations 1 and 12 practically no change has taken place, whereas between stations 12 and 30 the ML properties are virtually unchanged, with the pycnocline depressed by approximately 60 m. Although the latter stations are 500 m apart, the apparent synoptic views presented should be interpreted with caution.

A unique mapping of the internal horizontal structure of the chimney is provided by the Seasoar as it was towed in approximately 20 m depth, sampling approximately every 10 cm, along six **E–W** tracks 4 km apart (Figure 2). A contour plot of in situ, T, S, and σ_t is presented in Plate 3, in which the high wavenumber variability has been filtered to emphasize the mesoscale structures. (A consecutive median filter of width 101 was applied, yielding a resolution of about 10 m.) Again, the general structure agrees with the previous observations. The relatively cold, fresh structures inside the core close to the northwestern rim stand out even clearer. Plate 3c shows that the core σ_t typically exceeds 28.016, with slightly higher values in the southwestern part ($\sigma_t \sim 28.022$).

The fine-scale tows also provide insight that was not possible from the 2.5-km-resolution tows. E.g., the warm and saline anomalies of ~5 km-scale seen at 1°E, 77.5° and 77.56°N in Plate 3 could be only marginally resolved during the previous profiling (Plate 2). Alternatively, the anomalies can have propagated from the east, with an implied speed of 5 km over a day or so. Third, the warm, saline feature, about 5 km wide, appearing at the southern boundary at about 0.4°E (Plate 3, upper and middle panels), is also missing in the previous data (Plates 2a,b). Although no definite conclusion can be drawn on the time scale and potential propagation on the observed structures on the 5-km scale, it is apparent that these features are characteristic of the dynamics of the rim of the chimney.

Submesoscale Structure

For a detailed view of the horizontal T–S structure the individual tracks from the constant depth survey are plotted in Figure 7. Considerable variability on the 1-5-km scale is evident, as is an apparent decorrelation between neighbouring tracks 4 km apart. The gradients are occasionally sharp, i.e., of the order 0.2°C over less than a kilometer (Figure 7c), and the northwestern rim is superposed by anomalies of the order 0.1°C on a few kilometre scale. In the other tracks it is also seen that temperature anomalies of the order 0.1°C

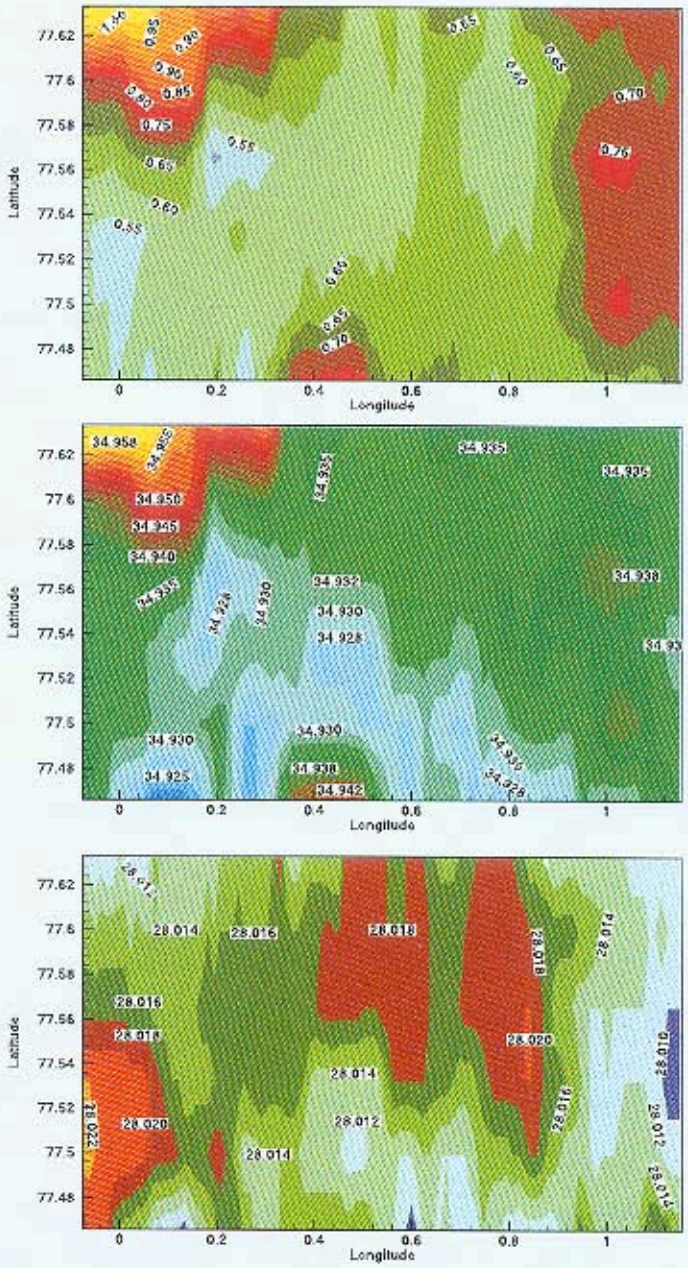

Plate 3. Horizontal plot of the scale tows. Temperature (upper) salinity (middle), sigma-t (lower). Data have been smoothed with a 101 point median filter prior to plotting.

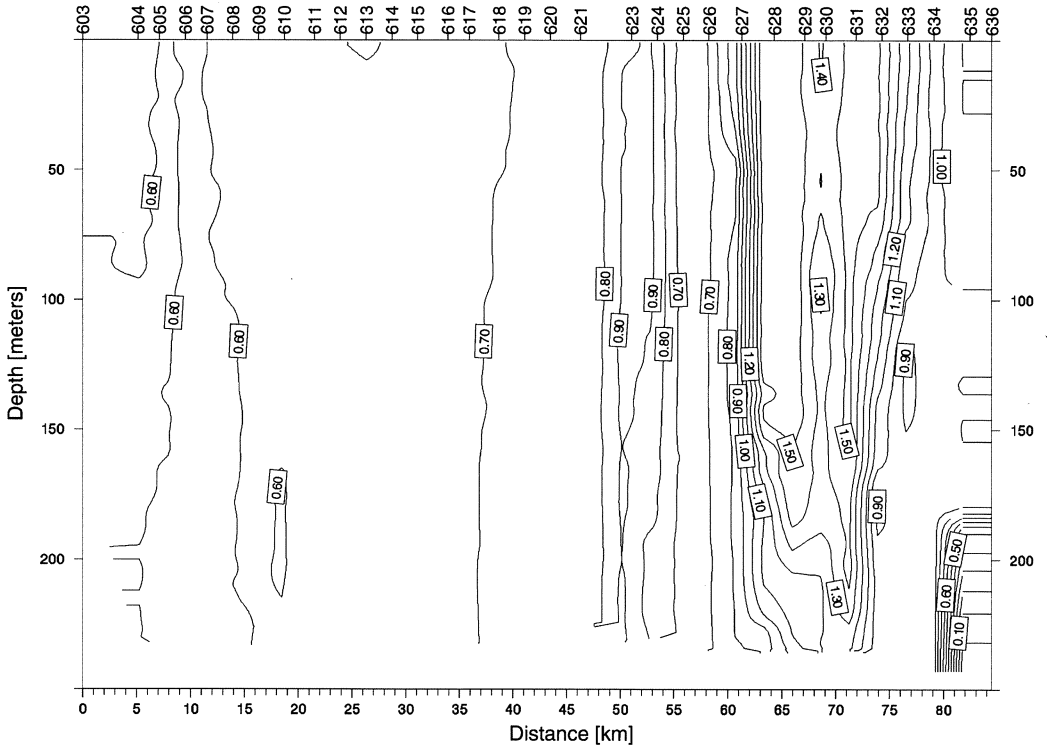

Figure 6. Seasoar Section 37, potential temperature. Contour interval is 0.1°C. The section is running W–E on Plate 2 at 77.52°N, extending further to the east, out of the panel.

over ~1 km is a common feature, i.e., comparable to the cross core temperature range revealed from the deep CTD sections (Figures 4a and 5a). A T–S scatter diagram (not shown) including the six tracks reveals an approximate linear fit between temperature and salinity with a slope of $\Delta T/\Delta S \simeq 20°C\ psu^{-1}$, a relation that is also apparent from the individual profiles. Thus, the salinity variability closely follows the temperature, consistent with linear mixing of the AW and the uAIW.

Numerical Experiment

To complement our understanding of the observed submesoscale variability, a numerical ocean model was set up to mimic the chimney interior. The model used is the MITgcm [*Marshall et al.*, 1997a,b] in its nonhydrostatic mode. The idealized model domain is 10 km × 10 km, representing the core of the chimney. It is doubly periodic in the horizontal and has a uniform depth of 3000 m, representative of the region. Initially, the fluid is motionless with small-amplitude random horizontal perturbations added to the stratification. The initial stratification is given by the potential density of Figure 3, related to the potential temperature through a linear equation of state, with a thermal expansion coefficient, $\alpha = 0.5 \times 10^{-4}\ (°C)^{-1}$. The hydrography was smoothed to remove the small-scale noise due to static instabilities. The numerical grid has a uniform horizontal resolution of 250 m and 32 vertical levels with spacing increasing smoothly from 20 m in the upper ocean to 200 m toward the seafloor. The internal radius of deformation (about 3 km) is thus well resolved. The same constant values were used for the Laplacian viscosity and diffusivity. The horizontal was set to $5\ m^2s^{-1}$ and the vertical to $0.02\ m^2s^{-1}$, values similar to those used by other authors, e.g., *Haine and Williams* [2002].

The heat flux from the ocean to the atmosphere was estimated from the field observations to be about 200 Wm^{-2}. The ML cooling from this is quite weak, as noted in the previous section. A value of 500 Wm^{-2} has previously been associated with convective chimneys and surface heat fluxes in the area [*Häkkinen*, 1988; *Häkkinen and Cavalieri*, 1989; *Johannessen et al.*, 1991]. The latter was therefore used to initiate convection in the numerical model, producing quite vigorous convection and some deepening of the mixed layer. After the first 20 days, the heat flux was smoothly reduced to the observed 200 Wm^{-2} for the remaining 30 days of the simulation.

The evolution of the vertical stratification is depicted in Figure 8. The horizontally averaged density is plotted for every second day. It shows that most of the ML deepening takes place during the first 20 days of relatively strong cooling. In the horizontal, distinct dense/light (cold/warm) anomalies of subduction/upwelling of 1-km scale emerge after about 1 day. (A power spectrum, not shown, revealed peaks at 0.7 and 1.4 km.) Although the deepening of the ML is quite marginal after day 20, the convective anomalies remain. Snapshots from day 30 of the density anomalies and the horizontal velocity and divergence at 20 m deep are shown in Plates 4a,b. The sinking regions are more intense than the upwelling, consistent with what has been inferred from observations and theory in general, cf. *Marshall and Schott* [1999].

The corresponding temperature difference between the cold and warm anomalies is typically 0.01-0.04°C, and the horizontal speed is 1-4 cms^{-1}. The spatial scale and temperature anomalies are quite consistent with the observed submesoscale variability (e.g., Figures 7a, e, k). Thus the present observations and numerical experiment suggest that there is a preference for convection to be organized at a kilometer scale, intermediate of the plume (see below) and the chimney scales. Similar patterns are also seen in the large-eddy simulations of *Garwood et al.* [1994], but the agreement may be partly coincidental. Although they are concerned with the high latitudes, their focus is thermobaric convection and the temperature anomalies that emerge are smaller than those reported herein.

The Plume Scale

The observed variability on the scale of a few hundred metres is also prominent, as can be most clearly seen in the temperature, ranging from about 0.02°C through 0.05°C (Figure 7). Hereafter we refer to this as the *plume scale*, since during active convection, plumes are expected to contribute to variability on this scale, as will be discussed below. Over all, the corresponding log-log plots of the power spectra for each section (not shown) revealed a linear decrease of energy with wavenumber, i.e. a "classical" turbulent cascade. However, on smaller scales than the kilometer scale there are marked deviations from this general pattern, especially demonstrated on Section 49, whose temperature profile is repeated in Plate 5a. Four distinct warm anomalies about 300 m wide, i.e. on the plume scale, are seen in the southwestern part of the chimney,

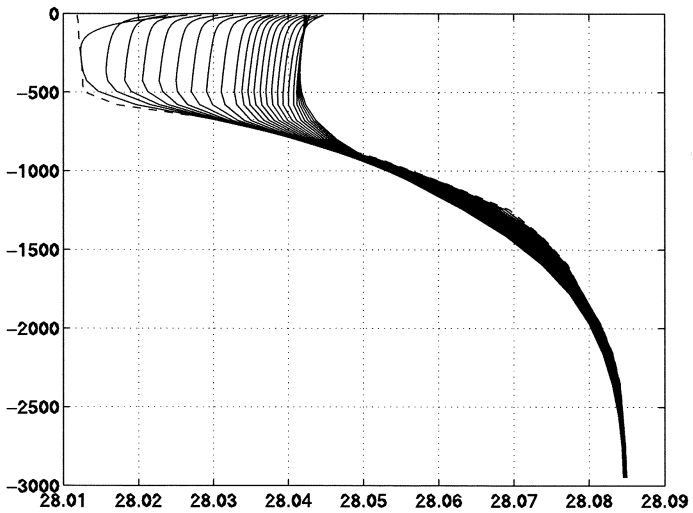

Figure 8. Modeled development of density [sigma units] versus depth [m] subject to a heat flux of 500 Wm^{-2} for the initial 20 days and 200 Wm^{-2} for the remaining 30. A curve is plotted every 2 days, starting with the dashed one.

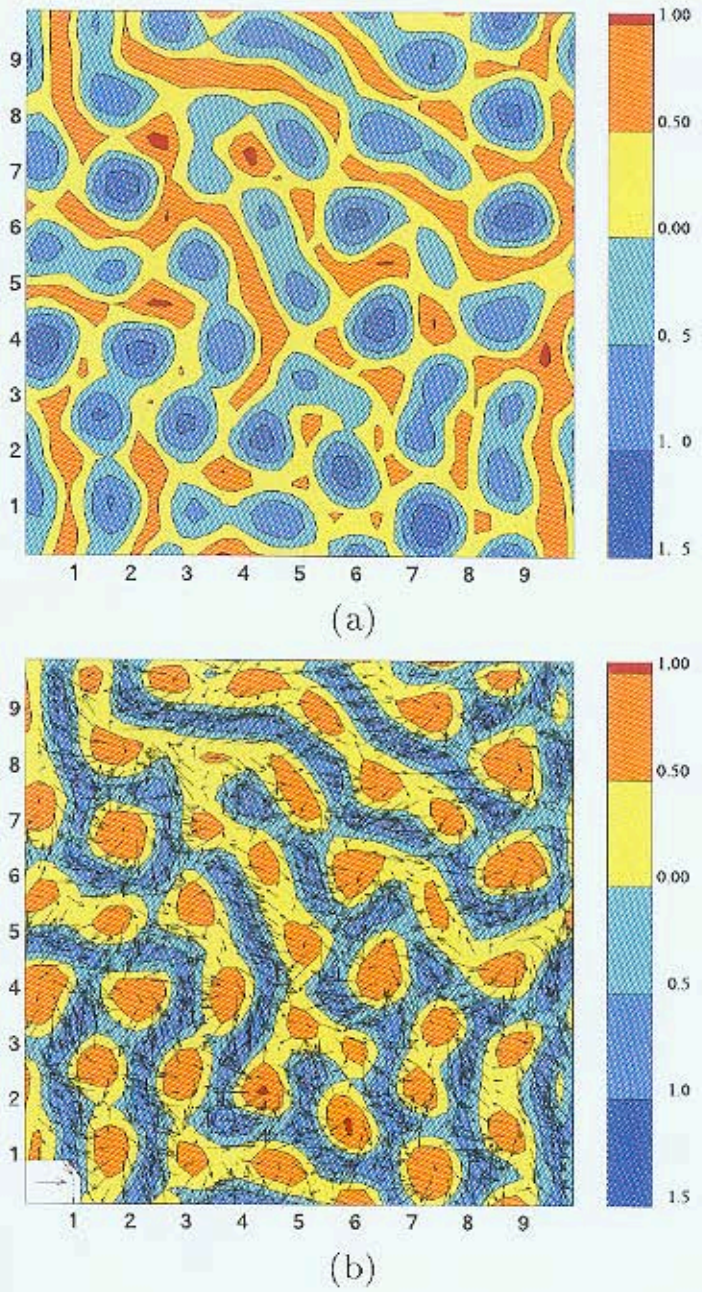

Plate 4. Model state in 20 m depth at $t = 30$ days for (a) density anomaly relative to 28.0405 kgm^{-3} and (b) horizontal divergence superimposed by velocity vectors (reference arrow 2 cms^{-1}. Units are [10^{-3} kgm^{-3}] in (a) and [10^{-4} s^{-1}] in (b). Co-ordinates in km.

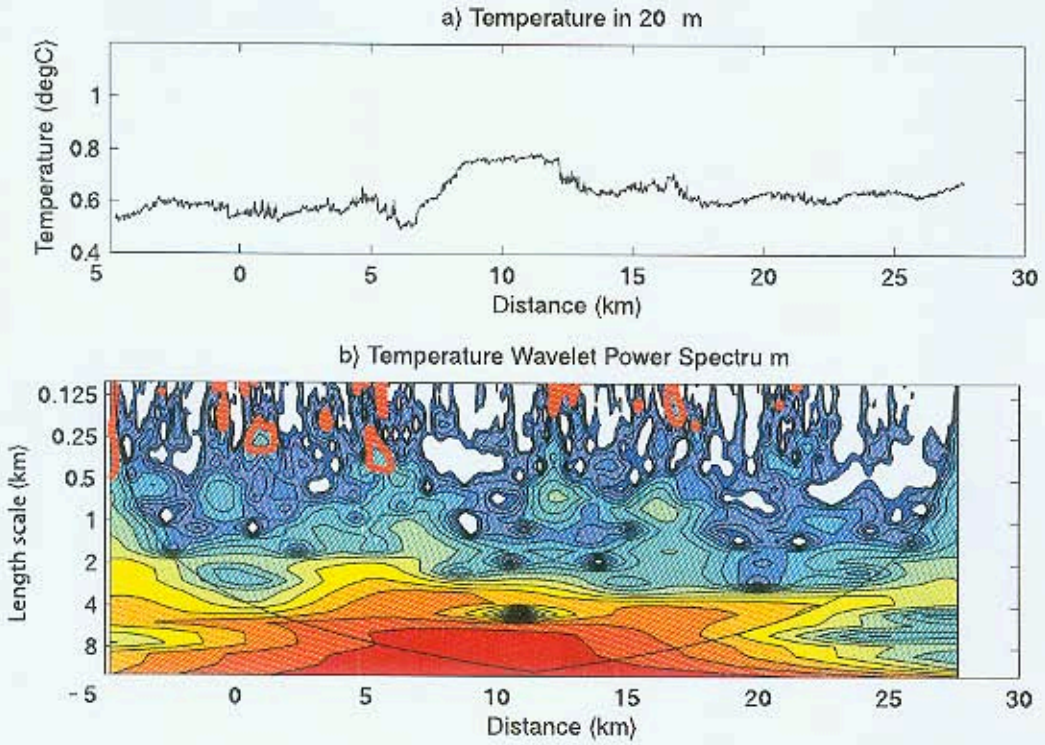

Plate 5. (a) Temperature profile along section 49 [°C] and (b) wavelet power spectrum of the same section as function of distance [km] (eastward from the 0° meridian) and length scale [km]. The color scale indicates relative variation of power with increasing levels from dark blue via green and yellow through red. Power is doubled for each color level. Thick red contours embrace regions where variability is significant at the 5% level. The four peaks between 0 and 2 km in (a), with corresponding maximum in power in (b), is described in the text.

i.e. between 0 and 2 km each with peaks of ~0.05°C above the background, i.e., comparable to the typical cross ML Q2 temperature variation of ~0.1°C. These may represent vertical motion. In a convective and otherwise cold environment, such warm anomalies are consistent with ascending warmer water masses compensating the sinking plumes.

Further quantification of the variability is provided by a wavelet power spectrum [*Kumar and FoufoulaGeorgiou*, 1997], shown in Plate 5b, in which the power is plotted as a function of distance along the track and length scale, again for Section 49 as an example. The signature of the aforementioned peaks clearly stands out both with elevated values on the plume scale and falling inside the region where variability is significantly different from noise, at the 5% level, denoted by the thick red contours in Plate 5b. A similarly significant region is seen to the east of 5 km, whereas the small regions on scales smaller than about 150 m are suspicious as the strength of the variability approaches the detection limit. Whether there exists a region of minimum power at about 500-m scale, indicative of a separation of scales on either side, is more speculative.

In order to check if there is any systematic variability of the energy on the plume scale, we examine the energy distribution on the band 150-400 m for the different profiles. We hereafter denote this quantity *Var*. Figure 9 shows there are significant peaks in *Var* on several profiles. In comparison with the raw profiles (Figure 7), these peaks are caused by impulse-like steps in the raw profiles, inducing energy on all scales. The marked exception is the first peak from the left on Section 49 (Figure 9), the previously described region, displaying marked locally increased levels of *Var*. In order to shed more light on this anomalous structure, we first quantify the effect of abrupt steps by computing $|\nabla T|$, evaluated over 1 km. The correlation of *Var* with, respectively, T, σ, and $|\nabla T|$ is shown in Table 1. Not surprisingly, high correlation of *Var* and $|\nabla T|$ is found on the northernmost Sections 44 and 45. Correlation between *Var* and σ is also relatively high on these sections, apparently due to the rim front, which is dominated by salinity. On Section 47 there is virtually no correlation between any of the quantities, probably because it is representative for the chimney interior, with minimal influence from the variability at the rim. The anomalous Section 49 shows a negative correlation between *Var* and T, whereas the other quantities show a positive or no correlation. Repeating the analysis for the westernmost portion of Section 49 by excluding the regions of the second *Var* peak and eastwards retains the high negative correlation between *Var* and T, but enhances the negative correlation between *Var* and σ, implying stronger influence of salinity. Furthermore, the correlation between *Var* and $|\nabla T|$ shows anomalous negative and high correlation, i.e. high variability for a more homogeneous background, which is contrary to the effect of abrupt property steps on the rim.

Taken together with the previous information from the deep CTD sections, we observe that the enhanced plume activity is consistent with increased mixing with the slightly cooler and fresher waters from beneath the ML. Whether the surface cooling is slightly stronger or the stratification slightly weaker than the background cannot be determined without further data. Probably it is a combination of both.

The plume scale appearing on Section 49 agrees well with a plume scale l determined from external parameters (*Marshall and Schott* [1999], Eq. 13a):

$$l = \left(\frac{B}{f^3}\right)^{1/2}$$

Using the turbulent heat flux ($Q = 200$ Wm^{-2}) to derive the buoyancy forcing B based on a representative value for the thermal expansion coefficient, $\alpha = 0.5 \times 10^{-4}(°C)^{-1}$, as for the ocean model, yields

$$B = 0.3 \times 10^{-7}\ \mathrm{m^2 s^{-3}}$$

and

$$l \simeq 100\mathrm{m}$$

Finally, an aspect of our observations perhaps linked to the microscale is worth mentioning. The sharp separation of the warm, saline ML water and the cold, fresh water beneath (Figure 3) is striking. The approximate property steps are $\Delta S = 0.05$ and $\Delta\theta = 0.75$°C. This stratification is opposite of what has been observed earlier [*Johannessen et al.*, 1991] and can potentially allow upward thermobaric convection.

DISCUSSION

Our observations of *Chimney94* indicate shallow convection over 400-600 m maintained by approximately 200 Wm^{-2} cooling at the surface. It can easily be shown that even if this flux works exclusively to cool the ML, it will take more than 3 months to erode the thermocline. In other words, deep-reaching convection is very unlikely during the remaining winter. Normally the heat flux in this area exceeds 500 Wm^{-2} [*Häkkinen*, 1988; *Häkkinen and Cavalieri*, 1989]. This often occurs in connection with cold Polar air outbreaks over warm water closer to the ice edge [*Buckley et al.*, 1979]. For such a flux the same deepening is obtained in only about 35 days. The 1994 winter also appeared to be warmer than normal for this area, implying less intense convection.

Despite the modest convective activity, a main finding is the evident horizontal variability on the submeso– and plume scales. In the chimney interior there are both in the observations (Figure 7) and in the numerical simulations (Plate 4) clear signatures of submesoscale anomalies. This suggests there are three distinct dynamical horizontal scales present:

The latter is probably because the surface forcing can operate slightly more effectively over a relatively thinner ML. Again, the modest forcing is taken as the reason why an unambiguous convection process was not observed with well-defined rim eddies in a more symmetric pattern.

Finally, we note the special stratification of the Boreas Basin, distingushing it from the Greenland Basin. In the former, the Atlantic derivative situated at the surface lies directly on top of the fresher and colder intermediate water, whereas in the Greenland Basin the stratification is "normal" with usually a low-salinity water at the surface [*Johannessen and Lygre*, 1996]. In a warm, saline over cold, fresh stratification, a parcel of intermediate water entrained into the convecting ML will become lighter than its surroundings and thus convect freely due to thermobaricity. Such "upward" convection is possible only in this atypical stratification and may serve as a significant mechanism for assisting convection in cases when the surface forcing is not powerful. It is striking that our observations show enhanced plume activity inside a cold and fresh submesoscale anomaly. A closer inspection of the role of the microscale processes is beyond the scope of the present study.

CONCLUSION

For the first time, a chimney has been investigated with a horizontal sampling interval down to 10 cm. *Chimney94* in the Boreas Basin in late winter 1994 was about 30 km in the zonal and 15 km in the meridional directions, the convection reaching typically 500 m. Within the core of the chimney the variability is notable on the submesoscale O(1 km) and the plume scale O(100 m). The latter scale—for the first time observed in this experiment—indicates active plume convection in agreement with theoretical considerations. A nonhydrostatic ocean model corroborates that convection can be organized on the submesoscale even under moderate forcing.

Strong activity on the rim of the chimney indicates that it is vulnerable to destabilisation, inhibiting its further development. Ambient anticyclones are not clearly discriminable from those associated with the rim process. Indications of augmented cooling inside rim cyclones is a sign of active, although weak, convection competing against the break up process. Finally, the special stratification with warm, saline water over cold, fresh water is shown to be a potentially important ingredient in the vertical exchange process.

NOMENCLATURE

B	buoyancy flux
H	thickness of the mixed layer
N	buoyancy frequency
R_d	Rossby radius of deformation
S	Salinity
T	in situ temperature
f	Coriolis parameter
l	length scale
α	thermal expansion coefficient of sea water
σ_θ	potential density anomaly
θ	potential temperature
ASW	Arctic Surface Water
AW	Atlantic Water
CTD	conductivity–temperature–depth
MIZEX	Marginal Ice Zone Experiment
ML	mixed-layer
SAR	Synthetic Aperture Radar
SIZEX	Seasonal Ice Zone Experiment
lAIW	lower Arctic Intermediate Water
uAIW	upper Arctic Intermediate Water

Acknowledgments. This EU ESOP project has been funded by the Norwegian Research Council as contribution to contract MAST2-CT93-0057 under the MAST-2 programme, the Nordic Council of Ministries, and Office of Naval Research. University of Bergen contributed with R/V *Håkon Mosby*. We thank the captain, crew, and scientific staff onboard R/V *Håkon Mosby* for splendid cooperation. Wavelet software was provided by C. Torrence and G. Compo and is available at URL: http://paos.colorado.edu/research/wavelets/ T.E. was supported by grants from the EU 5th Framework Programme project TRACTOR (contract EVK2-CT-2000-00080) and the Norwegian Research Council project ProClim (155923/700). Comments from two anonymous reviewers were helpful in improving the manuscript.

REFERENCES

Aagaard, K., E. Fahrbach, J. Meincke, and J.H. Swift, Saline outflow from the Arctic Ocean: its contribution to the deep waters of the Greenland, Norwegian and Iceland seas, *J. Geophys. Res.*, 96(C11), 20433-20441, 1991.

Alekseev, G., O.M. Johannessen, A. Korablev, V. Ivanov, and D. Kovalevsky, Interannual variability of water masses in the Greenland Sea and adjacent areas, *Polar Research*, 20, 201-208, The Sverdrup Symposium special issue, 2001.

Alekseev, G.V., O.M. Johannessen, A.A. Korablev, and A.Y. Proshutinsky, Arctic Ocean and sea ice, in *Arctic Environment Variability in the Context of Global Change*, edited by Bobylev, L.P., K.Y. Kondratyev, and O.M. Johannessen, pp. 107-202, Springer–Praxis books in environmental sciences, 2003.

Buckley, J.R., T. Gammelsrød, J.A. Johannessen, O.M. Johannessen, and L.P. Røed, Upwelling: Oceanic structure at the edge of the Arctic ice pack in winter, *Science*, 203, 165-167, 1979.

Budéus, G., Winter convective events and bottom water warming in the Greenland Sea, *J. Geophys. Res.*, 103(C9), 18513-18527, 1998.

Carmack, E., Large-scale physical oceanography of polar oceans, in *Polar oceanography. Part A physical science*, edited by Smith, W.O., pp. 171-222, Academic Press, 1990.

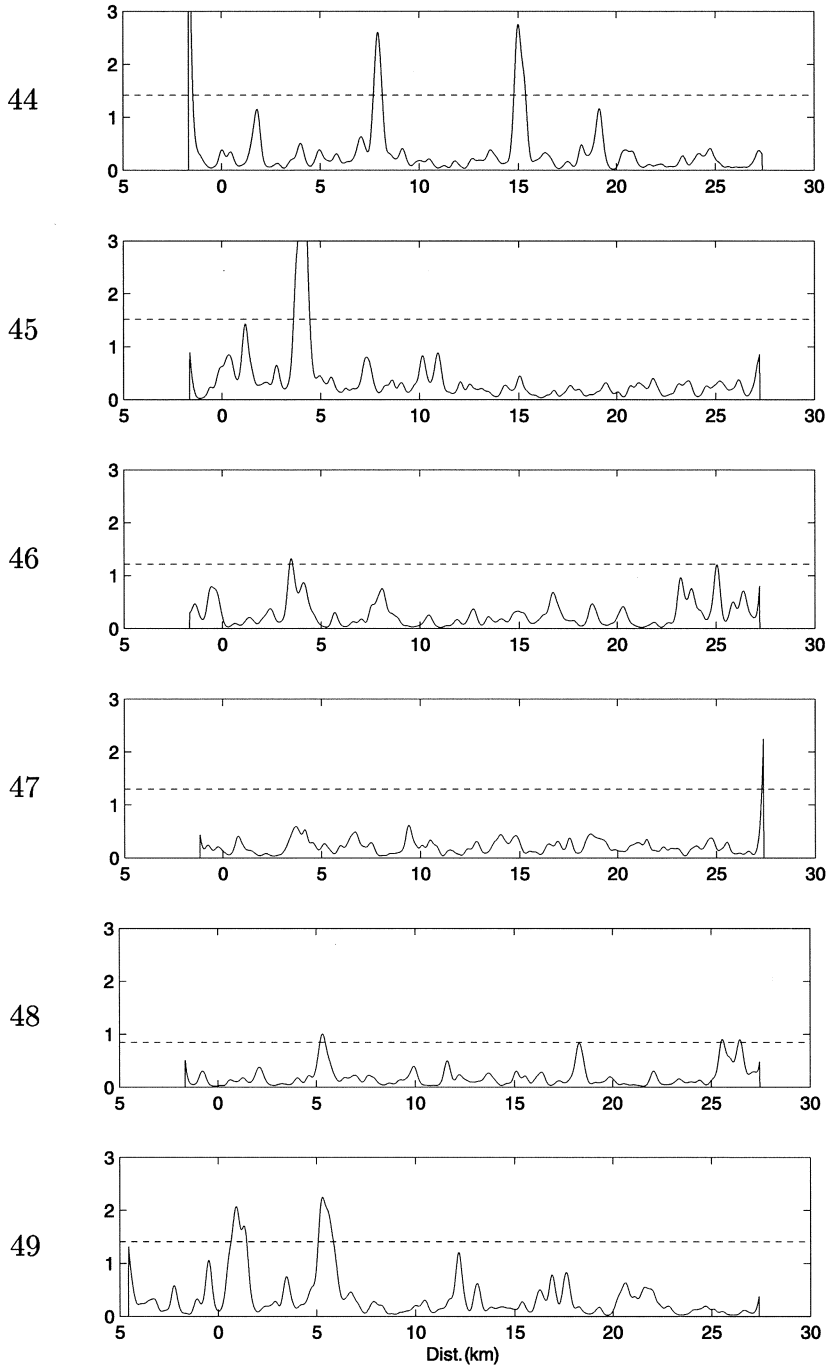

Figure 9. Along-track distribution of temperature variance [10^{-4} (°C)^2] on the 150-400 m scales from the fine-scale tows. The 95% confidence level is indicated with dashed lines. The ordinate has the same range for each plot to improve comparison.

Table 1. Correlation Between Various Parameters for the Fine-Scale Tows. *Var* denotes the temperature variance on the 150-400-m scales, T is temperature, σ density, and $|\nabla T|$ the absolute value of the temperature gradient computed over 1 km. Section 49 west denotes the portion west of 5 km in Plate 5.

Section	*Var* vs. T	*Var* vs. σ	*Var* vs. $\|\nabla T\|$
44	0.08	0.12	0.51
45	0.24	0.33	0.81
46	0.21	0.06	0.27
47	0.05	0.00	–0.01
48	0.20	0.08	–0.02
49	–0.30	–0.06	0.15
49 west	–0.26	–0.18	–0.17

the chimney (or meso), the submeso–, and the plume scales. This is in line with the ordering described by Marshall and Schott [1999] for the Labrador and Greenland seas, but with the important difference that they lack the intermediate scale of the present study, the submesoscale.

The observed concentration of energy on the 100-m horizontal scale, the plume scale, coincides with the width of vertically convecting plumes in agreement with several numerical studies and theoretical considerations [*Thorkildsen and Haugan*, 1999; *Marshall and Schott*, 1999]. Furthermore, remote sensing observations in the Greenland Sea by *Carsey and Roach* [1994] also point to a plume scale of 100 m, with a separation between plumes of about 300 m. We thus conclude that our observations show plume activity. More investigations are needed to clarify the important interactions between the various spatial scales.

Also notable is the irregular shape of the rim of the chimney, indicating substantial activity by meanders or eddies, eroding the chimney from the sides, i.e., a restratification process (Plate 2). On the other hand, in the north, the θ–S structure suggests slightly enhanced mixing with the underlying water, where there is also maximum cyclonic shear and the pycnocline is elevated (Figure 4). In this case a cyclone of the destabilized rim current thus moderately assists convection. Taking our observations, modeling, and previous work together, the state of the chimney—the ML depth and the horizontal extent of the chimney—reflects a dynamical balance in which the cooling is the process supporting convection and the erosion by the warm intrusions from the Atlantic domain is the destructive process. With a stronger cooling during the winter one should expect deeper reaching convection and an expansion of the convective region.

In contrast to *Chimney94*, *Chimney89* (also observed in the Boreas Basin by *Johannessen et al.*, [1991]) was more well defined. It was by itself colder as it was located closer to the ice edge and exposed to colder air masses typical of the winter of 1989. Perhaps more important is its deep structure with high salinities (34.92), indicating deep water in the core and surrounded by relatively saline lAIW. In the same area deep water was also observed at the surface in several O (10-km) chimney-like structures. Upper ocean chimneys observed 2 years earlier in 1987, discussed by *Johannessen et al.*, [1991], consisted of lAIW but lacked the deep-water core as for the 1989 observation. The more marked presence of deep water in the chimney structures in 1989 relative to 1987 may indicate a gradual renewal of the deep-water mass between these years.

The observations from 1987 and 1989 suggest that some preconditioning by lifting the lAIW to the surface is necessary for a deep-reaching chimney to form. Such a mechanism may be Ekman pumping or a cyclonic eddy, as discussed elsewhere [*Johannessen et al.*, 1991; *Killworth,* 1979]. However, the very small bottom-to-surface density difference, reported to be 0.02-0.03 sigma-units by *Johannessen et al.*, [1991], is probably also a reflection of the preexisting structure of the deep and intermediate waters [*Budéus*, 1998]. In contrast, in 1994 the intermediate waters (500-1000 m) consist of a much fresher uAIW ($S \sim 34.88$) and the bottom-to-surface density difference is 0.07 sigma-units (Figure 3), making penetration by surface convection unlikely, as discussed previously. The inverted hydrography compared to the earlier observation, with a slight capping by warm, saline AW, may also be due to the more eastern location of *Chimney94*.

According to *Gascard* [1990] 20 chimneys can account for a major part of intermediate and deep-water formation in the world ocean. In order to quantify the integral effect of the chimneys in the Greenland Sea, one has to estimate their number and lifetimes in addition to their vertical and horizontal structure. A key issue is the role of baroclinic eddies associated with the rim of the chimney. Is their major role in the postconvective process [*Marshall and Schott*, 1999], or do they also play an active role in the convection process [*Killworth*, 1979; *Straneo and Kawase*, 1999; *Eldevik and Drange*, 2002; *Gascard, et al.*, 2002; *Wadhams, et al.*, 2002]? Without being conclusive, our results definitely add more complexity to the picture: Apart from the rich submesoscale and finer internal structure inside the chimney described above, there are fronts and large (15-km) anticyclones in the ambient water, obscuring the separation of chimney core and exterior. Structures at the rim of the chimney entangle T–S signatures of water masses from the exterior (warm, saline) and the chimney core (cold, fresh).

Strikingly, the densest near-surface water occurred on the rim of the chimney, with the lightest, warmer, saltier water located only 2.5 km away. The dense water anomaly also coincided with a strong cyclonic shear, a maximum elevation of the pycnocline, and a slightly larger cooling of 0.05°C.

Carsey, F.D., and T. Roach, Oceanic convection in the Greenland Sea Odden region as interpreted in satellite data, in *Nansen Centennial Volume: The role of the Polar oceans in shaping the global climate*, edited by Johannessen, O.M., R. Muench, and J. Overland, pp. 211-222, American Geophysical Union Monograph, 1994.

Eldevik, T., and H. Drange, Resolved and parameterized convective eddies in the Greenland Sea, in *Norwegian Ocean Climate Project, Technical Report No. 3*, edited by Sætre Hjøllo, S., pp. 41-44, Geophysical Institute, University of Bergen, Bergen, Norway, 2002.

Garwood, R.W., S.M. Isakari, and P.C. Gallacher, Thermobaric convection, in *Nansen Centennial Volume: The role of the Polar oceans in shaping the global climate*, edited by Johannessen, O.M., R. Muench, and J. Overland, pp. 199-210, American Geophysical Union Monograph, 1994.

Gascard, J.C., Deep Convection and Deep Water Formation: Progress and Directions, *Eos, Transactions*, 71(49), 1837-1839, 1990.

Gascard, J.C., Open ocean convection and deep water formation revisited in the Mediterranean, Labrador, Greenland and Weddell Seas, in *Deep convection and deep water formation in the oceans*, edited by Chu, P.C., and J.C. Gascard, pp. 157-182, Elsevier, 1991.

Q4 Gascard, J.-C., A.J. Watson, M.J. Messias, K.A. Olsson, T. Johannessen, and K. Simonsen, Long-lived vortices as a mode of deep ventilation in the Greenland Sea, *Nature*, 416, 525-527, 2002.

Haine, T.W.N., and P. Williams, The role of non-hydrostatic dynamics in controlling development of a surface ocean front, *Ocean Modell.*, 4, 121-135, 2002.

Häkkinen, S., A note on chimney formation in ice edge regions, *J. Geophys. Res.*, 93(C7), 8279-8282, 1988.

Häkkinen, S., and D.J. Cavalieri, A study of surface heat fluxes in the Greenland, Norwegian, and Barents Seas, *J. Geophys. Res.*, 94(C5), 6145-6157, 1989.

Johannessen, J.A., O.M. Johannessen, E. Svendsen, R. Shuchman, T. Manley, W.J. Campbell, E.G. Josberger, S. Sandven, J.C. Gascard, T. Olaussen, K. Davidson, and J. VanLeer, Mesoscale eddies in the Fram Strait marginal ice zone during the 1983 and 1984 Marginal Ice Zone Experiments, *J. Geophys. Res.*, 92(C7), 6754-6772, 1987a.

Johannessen, O.M., V. Jensen, T. Lerøen, and K. Lygre, Data report on the Greenland Sea convective chimney experiment 1994, Special report 36, Nansen Environmental and Remote Sensing Center, 1995.

Johannessen, O.M., J.A. Johannessen,, J. Morison, B. Farrelly, and E. Svendsen, Oceanographic conditions in the marginal ice zone north of Svalbard in early fall 1979 with an emphasis on mesoscale processes, *J. Geophys. Res.*, 88, 2755-2769, 1983.

Johannessen, O.M., J.A. Johannessen, E. Svendsen, R. Shuchman, W.J. Campbell, and E.G. Josberger, Ice-edge eddies in the Fram Strait marginal ice zone, *Science*, 236, 427-429, 1987b.

Johannessen, O.M., and K. Lygre, Observations of convective chimneys, in *European Subpolar Ocean Programme, Sea Ice - Ocean Interactions*, edited by Wadhams, P., J.P. Wilkinson, and S.C.S. Wells, pp. 262-294, Commission of the European Communities, 1996.

Johannessen, O.M., S. Sandven, and J.A. Johannessen, Eddy-related winter convection in the Boreas Basin, in *Deep convection and deep water formation in the oceans*, edited by Chu, P.C., and J.C. Gascard, pp. 87-105, Elsevier, 1991.

Killworth, P.D., On "Chimney" formations in the ocean, *J. Phys. Oceanogr.*, 9, 531-554, 1979.

Kumar, P., and E. Foufoula-Georgiou, Wavelet analysis for geophysical applications, *Rev. Geophysics*, 35, 385-412, 1997.

Legg, S., and J. Marshall, A heton model of the spreading phase of open-ocean deep convection, *J. Phys. Oceanogr.*, 23, 1040-1056, 1993.

Marshall, J., A. Adcroft, C. Hill, L. Perelman, and C. Heisey, A finite volume, incompressible Navier Stokes model for studies of the ocean on parallel computers, *J. Geophys. Res.*, 102, C3, 5753-5766, 1997a.

Marshall, J., C. Hill, L. Perelman, and A. Adcroft, Hydrostatic, quasi hydrostatic, and non-hydrostatic ocean modeling, *J. Geophys. Res.*, 102(C3), 5733-5752, 1997b.

Marshall, J., and F. Schott, Open-ocean convection: observations, theory and models, *Rev. Geophysics*, 37, 1-64, 1999.

MEDOC-group, Observation of formation of deep water in the Mediterranean Sea, *Nature*, 227, 1037-1040, 1970.

MIZEX-group, The winter Marginal Ice Zone Program in the Fram Strait/Greenland Sea, *EOS, Trans. Amer. Geophys. Union*, 70, 545-555, 1989.

Pedlosky, J., *Geophysical Fluid Dynamics*, Springer, New York, 1979.

Sandven, S., O.M. Johannessen, and J.A. Johannessen, Mesoscale eddies and chimneys in the marginal ice zone, *J. Mar. Syst.*, 2, 195-208, 1991.

Send, U., and J. Marshall, Integral effects of deep convection, *J. Phys. Oceanogr.*, 25, 855-872, 1995.

SIZEX-group, SISEX 89 Experiment Report, Technical Report 23, Nansen Remote Sensing Center, 1989.

Straneo, F., and M. Kawase, Comparisons of localized convection due to localized forcing and to preconditioning, *J. Phys. Oceanogr.*, 29, 55-68, 1999.

Thorkildsen, F., and P.M. Haugan, Modeling of deep water renewal through cold convective plumes, *Deep-Sea Res. II*, 46, 1357-1383, 1999.

UNESCO, The Practical Salinity scale 1978 and the International Equation of State of Seawater 1980, *Techn. Pap. in Mar. Sci.*, 36, UNESCO, 1981.

UNESCO, Algorithms for computation of fundamental properties of seawater, *Techn. Pap. in Mar. Sci.* 44, UNESCO, 1983.

Wadhams, P., J. Holfort, E. Hansen, and J.P. Wilkinson, A deep convective chimney in the winter Greenland Sea, *Geophys. Res. Lett.*, 29, DOI 10.1029/2001GL014306, 2002.

Watson, A.J., M.J. Messias, E.F.K.A. Van Scoy, T. Johannessen, K.I.C. Oliver, D.P. Stevens, F. Rey, T. Tanhua, K.A. Olsson, F. Carse, K. Simonsen, J.R. Ledwell, E. Jansen, D.E. Cooper, J.A. Kruepke, and E. Guilyardi, Mixing and convection in the Greenland Sea from a tracer-release experiment, *Nature*, 401, 902-904, 1999.

T. Eldevik, O.M. Johannessen, and K. Lygre, Nansen Environmental and Remote Sensing Center, Thormøhlensgate 47, N-5006 Bergen, Norway. (tor.eldevik@nersc.no; ola-johannessen@nersc.no; kjetil.lygre@nersc.no)